

Using spatial partitioning to reduce the bit error rate of diffusion-based molecular communications

Muhammad Usman Riaz, Hamdan Awan, Chun Tung Chou, *Member IEEE*

Abstract

This work builds on our earlier work on designing demodulators for diffusion-based molecular communications using a Markovian approach. The demodulation filters take the form of an ordinary differential equation (ODE) which computes the log-posteriori probability of observing a transmission symbol given the continuous history of receptor activities. A limitation of our earlier work is that the receiver is assumed to be a small cubic volume called a voxel. In this work, we extend the maximum a-posteriori demodulation to the case where the receiver may consist of multiple voxels and derive the ODE for log-posteriori probability calculation. This extension allows us to study receiver behaviour of different volumes and shapes. In particular, it also allows us to consider spatially partitioned receivers where the chemicals in the receiver are not allowed to mix. The key result of this paper is that spatial partitioning can be used to reduce bit-error rate in diffusion-based molecular communications.

Index Terms

Molecular communications; Demodulation; Maximum a-posteriori; Spatial partitioning; Bit error rate.

I. INTRODUCTION

MOLECULAR communication is an emerging field which focuses on realizing communication between nano-scale devices [1], [2] and especially the internet of bio-nano things [3]. A key characteristic of molecular communication is the use of molecules as the information carrier. This paper considers diffusion-based molecular communications [4][5].

The receiver is an important component in any communications system. We can divide the techniques for improving receiver performance of diffusion-based molecular communications into two categories. The first category of work uses signal processing techniques. Some examples in this category are: the

M. Usman Riaz and C.T. Chou are with the School of Computer Science and Engineering, The University of New South Wales, Sydney, New South Wales 2052, Australia. Hamdan Awan is with Department of Electrical Engineering and Computer Science, York University, Toronto, Canada. Emails: usmanriaz@cse.unsw.edu.au, c.t.chou@unsw.edu.au, hawan@eecs.yorku.ca

paper [6] designs a receiver based on minimum mean square error method; [7] uses multiple samples per symbol and maximum likelihood method to design a receiver; [8] designs a matched filter to maximise the signal-to-interference-plus-noise ratio; [9] studies the design of estimate-and-forward relay nodes; and, [10] uses data fusion of decisions from multiple receivers.

The second category of work uses physical or chemical properties to improve communications performance. Some examples are: [11] uses enzyme in the medium to reduce interference; [12] uses flow to improve the performance of the weighted sum detector at the receiver; [13] uses chemical reactions in the transmission medium to reduce interference.

This paper proposes to use the physical mechanism of spatial partitioning to improve communication performance. Our work is inspired by the fact that receptors on the cell membrane are organized into spatially separated clusters of receptors [14]. In this paper, we assume that the receiver uses receptors which can be activated by the signalling molecules. We propose to segregate these receptors into a number of clusters separated spatially. We consider two configurations: partitioned and mixed. In the partitioned configurations, spatial isolation is perfect and receptors cannot move between clusters; however, in mixed configurations, receptors can diffuse between the clusters. For both configurations, we derive the maximum-a-posteriori (MAP) demodulator by leveraging our earlier work on designing demodulators for diffusion-based molecular communications using a Markovian approach [15][16].

This paper also removes a limitation of our earlier work in [15][16] where the receiver is assumed to be a small cubic volume called a voxel. In this paper, we assume that the receiver consists of multiple voxels and the union of these voxels define the shape of the receiver. This method of modelling a 3-dimensional volume is similar to that in finite difference method. In this paper, we extend the method of demodulator design in [15][16] to the multi-voxel case.

The contributions of this paper are:

- We propose to use spatial partitioning to reduce the bit error rate (BER) of diffusion-based molecular communications.
- We derive the MAP demodulator for both the partitioned and mixed configurations. This derivation of the MAP demodulator applies to a receiver with multiple voxels.
- We use our derived demodulators to demonstrate that the partitioned receiver has a lower BER compared with the mixed configuration. We also show that our demodulator for the mixed configuration can offer gradual degradation in BER from the partitioned configuration.
- We demonstrate that we can reduce BER by using a receiver which has a larger number of voxels.

The rest of the paper is organized as follows. Section II discusses the related work. In Section III we present the background and a summary of our previous work in [15][16]. Section IV presents MAP demodulator for the partitioned and mixed configurations. Section V presents numerical studies on comparing the performance of the partitioned and mixed configurations. Finally, Section VI concludes the paper.

II. RELATED WORK

A number of insightful surveys have been written on the topic of molecular communications, see [1], [2], [17], [18], [4].

There are three main components of a molecular communications system, namely transmitter, propagation medium and receiver. For molecular communications transmitters, many different modulation methods have been proposed. These include Molecule Shift Keying, Frequency Shift Keying, on-off keying and Concentration Shift Keying [19], [20], [21]. In this paper, our transmitter uses Reaction Shift Keying (RSK) which is proposed in our earlier work [16], [15], [22] [23]. In RSK, the transmission symbols are generated by a set of chemical reactions and are characterised by the time-varying concentration of the signalling molecules.

For the modelling of the propagation medium, various models have been proposed in literature. A common model is to assume that space is continuous, see e.g. [24], [25], [26], [11], [13]. In this paper, we assume that the medium is divided into voxels [27], [28], [29]. The voxel based setting allows us to model the molecular communication networks, which consist of both diffusion and chemical reactions, by using the reaction-diffusion master equation (RDME).

In Section I, we discussed two categories of work on improving receiver performance. Another method to classify different receivers that have been used in molecular communication is: those that use chemical reactions at the receiver, e.g. [30], [31], [32], [33], [34], and those that do not, e.g. [35], [36], [37], [21]. In this work, we assume that the receiver uses chemical reactions at the receiver.

The demodulation problem considered in this paper can be considered as using data fusion to combine the measurements coming from multiple voxels in order to carry out demodulation. Data fusion has previously been considered in molecular communications in [10]. The paper [10] assumes that there are multiple receivers; each receiver makes a hard decision for ON-OFF keying and a fusion centre makes an overall decision based on the decisions from the receivers. This paper uses a different method for data fusion. For our proposed demodulator, each voxel computes an approximate log-posteriori probability and we add these probabilities up to obtain the log-posteriori probability of the receiver.

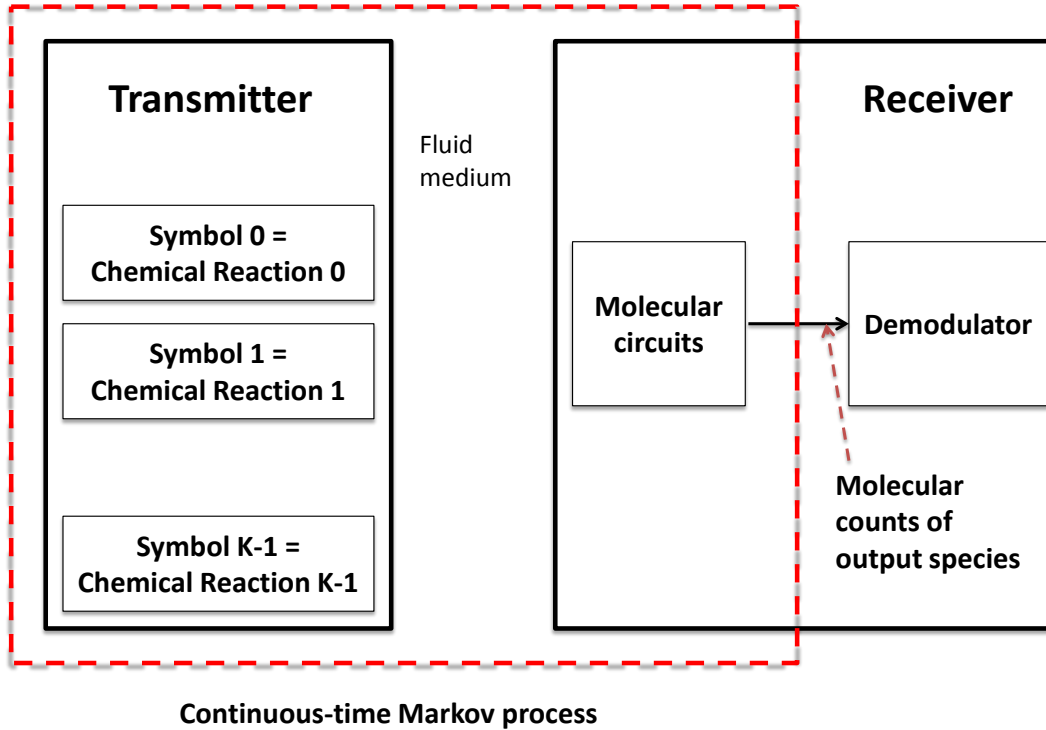


Fig. 1. System Overview.

In this paper, we consider using spatial partitioning to reduce the BER in molecular communications. Spatial partitioning has been studied in biophysics, e.g. the authors of [14] study how spatial partitioning can reduce noise, and the paper [38] studies the impact of receptor clustering on the noise in cell signalling. In the area of chemical based computation, the authors of [39] use partitioning to improve the performance of a molecular computing system. In our previous paper [40] we study the impact of partitioning on the variance of output signal. In [40], our conclusion is that partitioning can be used to reduce the variance of output signal but no receiver mechanisms have been proposed.

III. BACKGROUND AND SUMMARY OF PREVIOUS WORK

This section provides a summary of our previous work in [15], [16] on using a Markovian approach to derive a MAP demodulator. This section is divided into two subsections. Section III-A presents the modelling framework while Section III-B presents the MAP demodulator.

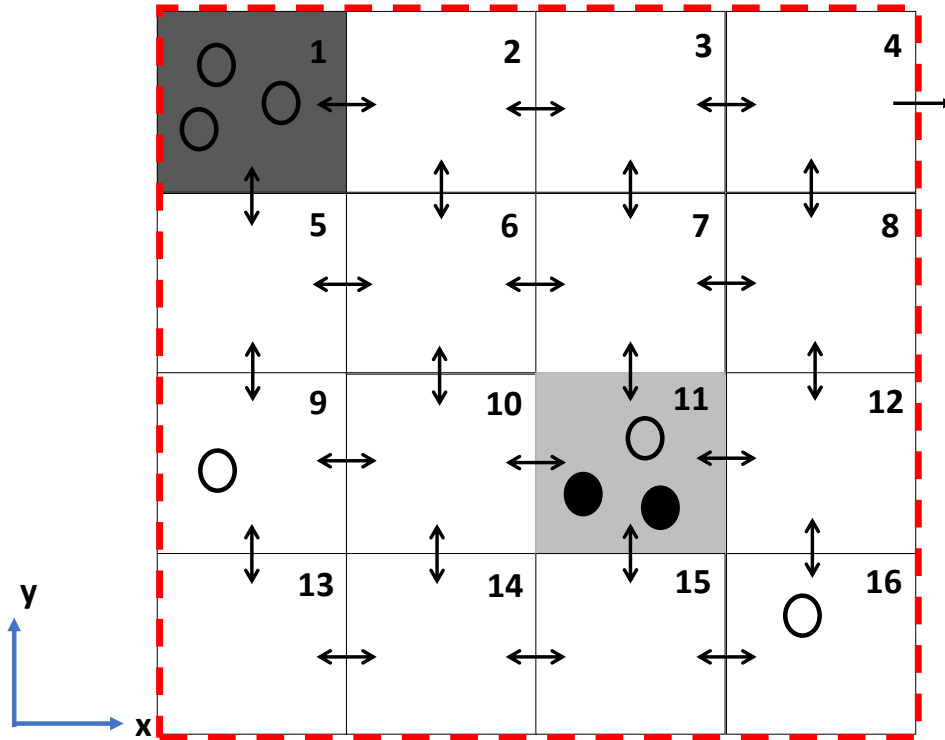


Fig. 2. The propagation medium is divided into voxels.

A. Modelling framework

In [15], [16], we consider a molecular communication system with a transmitter and a receiver inside a fluid propagation medium. Fig. 1 shows an overview of the system. We assume that the transmitter and the receiver communicate with one type of signalling molecules denoted by S . We will now discuss the modelling of the system components in further details.

1) *Propagation medium*: Signalling molecules diffuse from transmitter to receiver through a propagation medium. We model the propagation medium as a rectangular prism. We divide the medium into voxels. This is the same as applying a finite difference spatial discretization to a volume. Fig. 2 shows a 2-dimensional projection of a medium consisting of 4-by-4-by-1 voxels. In order to facilitate the description later on, we index each voxel by using integers 1,...,16 which are shown in the top-right corner of each voxel. We model the diffusion of the signalling molecules by using spatially discrete jumps between neighbouring voxels. For example, a signalling molecule in Voxel 1 in Fig. 2 can diffuse to any of its neighbouring voxels, which are Voxels 2 and 5. The double headed arrows in Fig. 2 show the direction of diffusion. We assume the diffusion of the signalling molecules are independent each other.

We assume the medium is homogeneous with a constant diffusion coefficient D for the signalling molecules. By applying a finite difference discretization to the 3-dimensional diffusion equation [41], it can be shown that within an infinitesimal time Δt , the probability that a signalling molecule will jump from a voxel to a neighbouring voxel is $\frac{D}{w^2} \Delta t$ where w denotes the length a voxel edge.

Lastly, our model can be used to model two types of boundary conditions: reflecting boundary condition where signalling molecules are not allowed to leave the medium; or, absorbing boundary condition where signalling molecules may leave the medium forever, e.g. the single headed arrow in Voxel 4 in Fig. 2 shows that signalling molecules may leave the medium.

2) *Transmitter*: The transmitter is assumed to occupy only one voxel. The role of the transmitter is to produce the signalling molecules for the transmission symbols. We assume that the transmitter uses RSK. This means that each symbol corresponds to a time-varying concentration profile of signalling molecules produced by a set of chemical reactions, Fig. 1 depicts a transmitter which can produce K different transmission symbols.

Once the signalling molecules have been produced by the transmitter, they are free to diffuse in the medium,

3) *Receiver*: In [15], [16], we assume that the receiver occupies one voxel, which is an assumption which we will change in Section IV of this paper. In this section, we follow the assumption in [15], [16].

We divide the operation of the receiver into two blocks, which we will refer to as the front-end and back-end blocks, see Fig. 1. The front-end block consists of a molecular circuit, which is another name for a set of chemical reactions. In [15], the front-end block is assumed to be a reversible ligand-receptor binding while in [16], the front-end block can be any molecular circuit. For example, the following molecular circuit is considered in [42]:



where g_+ and g_- are propensity function constants; and X and X_* are, respectively, the inactive and active forms of a species. Reaction (1a) is an activation reaction where the signalling molecule S turns inactive X into active X_* , while Reaction (1b) is a deactivation reaction.

Note that Table I contains a list of commonly used constants and chemical symbols for easy referral.

One or more chemical species in the front-end molecular circuit are chosen as the output species. The molecular counts of the output species over time are the output signals of the front-end, which are fed into the back-end as the input signals, see Fig. 1. The back-end of the receiver is the demodulator whose

aim is to infer the symbol that the transmitter has sent by using the input signals to the demodulator, i.e. the molecular counts of the output species of the front-end molecular circuit.

B. MAP demodulator

This section summaries the steps of deriving the MAP demodulator in our Markovian framework [15], [16]. For illustration, we assume that the front-end molecular circuit of the receiver is given by Reactions (1). We further assume that the molecules X and X_* can only be found in receiver voxels, and they are uniformly distributed in the voxel. We also assume that the total number of X and X_* molecules is a constant M . We designate X_* as the output species. Let $x(t)$ and $x_*(t)$ denote, respectively, the *number* of X and X_* molecules at time t . Note that both $x(t)$ and $x_*(t)$ are piece-wise constant because they are molecular counts.

We model the transmitter, medium and receiver front-end by using a RDME [41]. Note that RDME is a specific type of continuous-time Markov process (CTMP). This means the signal $x_*(t)$ is a realization of a CTMP.

Remark 1: Note that RDME assumes that space is discretised into voxels and time is continuous, therefore RDME is compatible with the discretisation of the medium discussed in Section III-A1. There is another rationale why we choose RDME. For the design of molecular communications systems, we need a stochastic model that can model systems with both diffusion and chemical reactions. There are three main classes of such models: Smoluchowski equation [43], RDME and the Langevin equation [44]. The Smoluchowski equation is based on particle dynamics. It is a fine grained model but hard to work with analytically. Both RDME and Langevin are easier to work with analytically but master equation has a finer scale and granularity compared to the Langevin equation [45]. Therefore we choose to use RDME which allows us to use the Markovian theory for analysis and is at the same time a finer grained model. Note that there is some recent work in combining the voxel-based approach (also known as the mesoscopic approach) and the Smoluchowski equation (also known as the microscopic approach) in simulating systems with both reactions and diffusion, see [46] and [47]. \square

Since X_* has been designated as the output species of the front-end molecular circuit, the signal $x_*(t)$ is available to the demodulator. For the derivation of the demodulation filter, we assume that at time t , the data available to the demodulation filter is $x_*(\tau)$ for all $\tau \in [0, t]$. We use $\mathcal{X}_*(t)$ to denote the continuous-time history of $x_*(t)$ up to time t .

We use the Bayesian framework for demodulation. Let $\mathbf{P}[k|\mathcal{X}_*(t)]$ denote the posteriori probability that symbol k has been sent given the history $\mathcal{X}_*(t)$. Instead of working with $\mathbf{P}[k|\mathcal{X}_*(t)]$, we will work with

its logarithm. Let $L_k(t) = \log(\mathbf{P}[k|\mathcal{X}_*(t)])$. Note that the log-posteriori probability diverges in continuous time, but we are able to compute a shifted version of it. For ease of reference, we will simply refer to the shifted version as the log-posteriori probability. We can use the method in [16] to show that we can compute $L_k(t)$ by using the following ordinary differential equation (ODE):

$$\begin{aligned} \frac{dL_k(t)}{dt} = & \left[\frac{dx_*(t)}{dt} \right]_+ \log(\mathbf{E}[n_R(t)|k, \mathcal{X}_*(t)]) - \\ & g_+(M - x_*(t))\mathbf{E}[n_R(t)|k, \mathcal{X}_*(t)] \end{aligned} \quad (2)$$

where $[\xi]_+ = \max(\xi, 0)$ and $\mathbf{E}[n_R(t)|k, \mathcal{X}_*(t)]$ is the estimation of the mean number of signalling molecules in the receiver voxel.

The computation of $\mathbf{E}[n_R(t)|k, \mathcal{X}_*(t)]$ requires extensive computation because it requires an optimal Bayesian filtering problem to be solved. In [15], we propose to replace the hard-to-compute $\mathbf{E}[n_R(t)|k, \mathcal{X}_*(t)]$ by $\mathbf{E}[n_R(t)|k]$, which is the mean number of signalling molecules if Symbol k is transmitted. Let $\sigma_k(t)$ denote $\mathbf{E}[n_R(t)|k]$. With the proposed replacement, Eq. (2) becomes:

$$\frac{dZ_k(t)}{dt} = \left[\frac{dx_*(t)}{dt} \right]_+ \log(\sigma_k(t)) - g_+(M - x_*(t))\sigma_k(t) \quad (3)$$

where $Z_k(t)$ is an approximation of $L_k(t)$. We can interpret Eq. (3) as using $\sigma_k(t)$ as an internal model or prior knowledge for demodulation. The use of internal model is fairly common in signal processing and communications, e.g. in matched filtering.

Note that Eq. (2) is the optimal solution for the demodulation problem. The replacement of $\mathbf{E}[n_R(t)|k, \mathcal{X}_*(t)]$ by $\mathbf{E}[n_R(t)|k]$ means that Eq. (3) is a sub-optimal solution. We show in [15] that $Z_k(t)$ from Eq. (3) approximates $L_k(t)$ in Eq. (2) well.

To make the decision at time t , the demodulator decide symbol \hat{k} is transmitted if $\hat{k} = \arg \max_{k=0, \dots, K-1} Z_k(t)$. Also, $Z_k(0)$ is initialized to the logarithm of the prior probability that the transmitter sends Symbol k . The structure of the demodulator is depicted in Fig. 3. The demodulator consists of K filters computing $Z_k(t)$ and a maximum block to determine the transmission symbol.

IV. RECEIVER WITH MULTIPLE VOXELS

This section derives the demodulator when the receiver consists of multiple voxels. We will consider both the partitioned and mixed configurations.

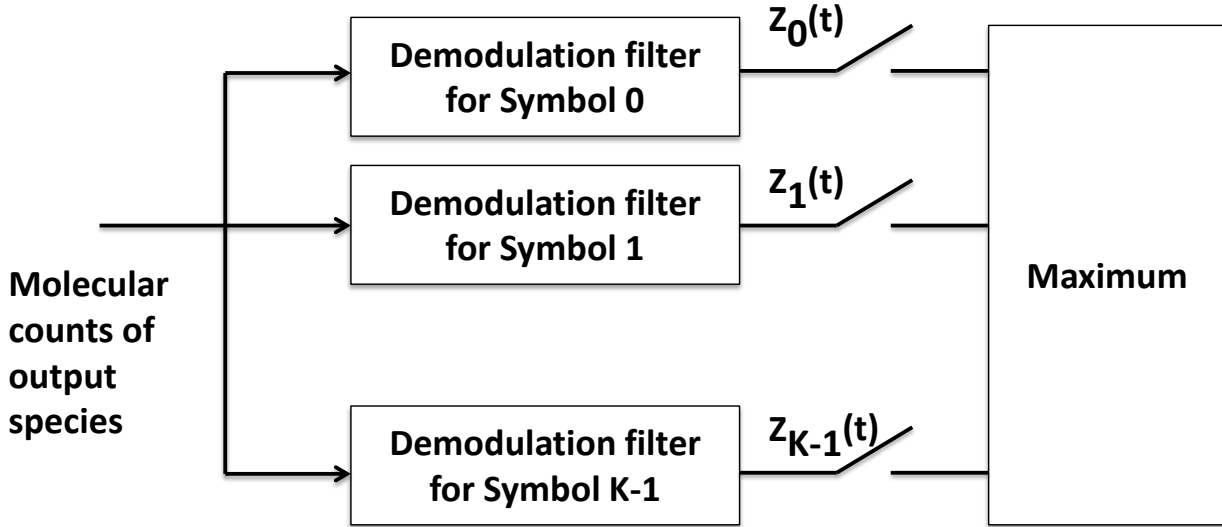


Fig. 3. The structure of the demodulator.

A. Multi-voxel receiver demodulation problem

We assume the receiver consists of P voxels where $P > 1$. Without loss of generality, we assume these P voxels form a connected volume. We will use p to index the voxels in the receiver, where $p = 1, \dots, P$. We will explain the demodulation problem using an example.

Example 1: In this example, we assume the molecular circuit (1) is present in all the P receiver voxels. We will continue to use the RDME to model the system. The RDME framework requires us to distinguish between the S , X and X_* in different voxels. We will use S_p , X_p and X_{*p} to denote the S , X and X_* in the p -th receiver voxel where $p = 1, \dots, P$. The P molecular circuits in the receiver voxels can be written

as:



We designate X_{*p} , for $p = 1, \dots, P$, as the output species of the receiver. Let $x_p(t)$ and x_{*p} denote respectively the number of X_p and X_{*p} molecules at time t . Let also $\mathcal{X}_{*p}(t)$ be the continuous history of the species X_{*p} up to and including time t . Our goal is to determine the posteriori probability $\mathbf{P}[k | \mathcal{X}_{*1}(t), \dots, \mathcal{X}_{*P}(t)]$ that the k -th transmitter symbol has been sent given the histories $\mathcal{X}_{*1}(t), \dots, \mathcal{X}_{*P}(t)$. \square

Note that it is possible to generalise the above examples in a few different ways: we can use molecular circuits other than (1); we can use different molecular circuits in different receiver voxels; we can use different choices of output species. We note that the methodology that we have developed to derive the demodulator can deal with all these generalisations.

We make the assumption that the species in the front-end molecular circuits (e.g. X and X_* in (1)) can only be found in the receiver. Also these species are confined within the receiver and cannot get into the propagation environment. In the text below, we will use the term receiver species to refer to these chemicals.

B. Mixed and partitioned configurations

Inspired by the study [14] which shows that spatial partitioning of the receptors on cell membrane can be used to reduce noise, we will consider two different configurations for the receiver.

For illustration, we assume the receiver consists of 4 voxels arranged in 2-by-2 configuration as shown in Fig. 4.

In the first configuration, which is illustrated in Fig. 4a, a receiver species is allowed to diffuse from a receiver voxel to another receiver voxel. We will refer to this configuration as mixed as the receiver species is allowed to mix among the receiver voxels.

In the second configuration, which is illustrated in Fig. 4b, a receiver species cannot move from a receiver voxel to another. In this case, we can assume the receiver voxel wall is a selective membrane which prevent certain species from moving between voxels. We will refer to this configuration as partitioned.

We will see shortly that the demodulators for the mixed and partitioning cases are different. Also, we will show in Section V that partitioned configuration has a lower BER compared to the mixed configuration.

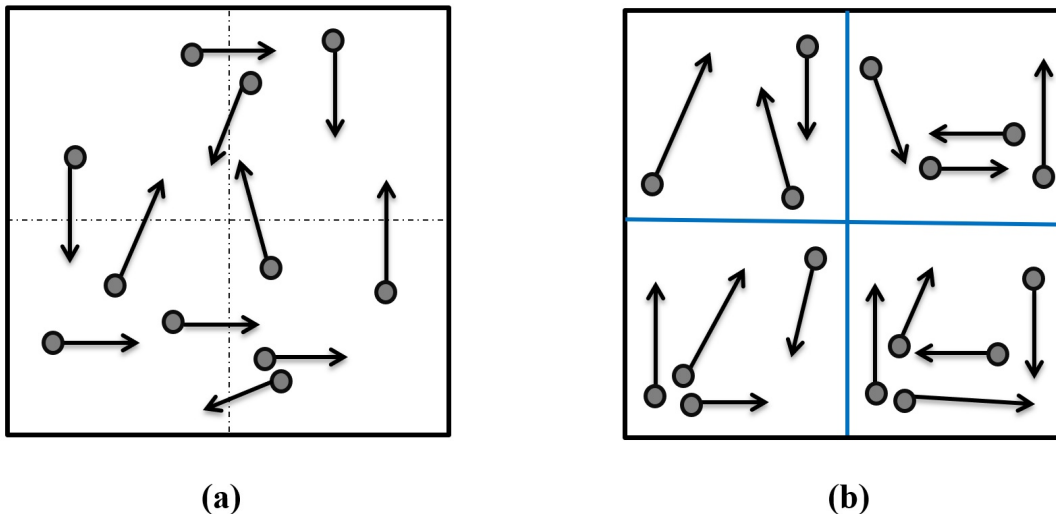


Fig. 4. (a) The mixed configuration. (b) The partitioned configuration.

We note that the voxel framework is well suited to model the partitioned and mixed configurations. This is because, for the voxel framework, it is possible to choose the value of the diffusion coefficient of a species between any two voxels. If a species is not allowed to pass between the interface of two voxels, then its diffusion coefficient for that interface is zero.

C. MAP demodulator for the partitioned configuration

In this section, we will derive the MAP demodulator for the demodulation problem illustrated in Example 1. In particular, in this section, we consider the partitioned configuration where the species X and X_* are not allowed to move among the receiver voxels. This means the total number of X and X_* molecules in a receiver voxel remains constant. We will use M_p to denote the total number of X and X_* molecules in the p -th receiver voxel.

The aim of the demodulation problem is to determine the posteriori probability $\mathbf{P}[k|\mathcal{X}_{*1}(t), \dots, \mathcal{X}_{*P}(t)]$ that the k -th transmitter symbol has been sent given the histories $\mathcal{X}_{*1}(t), \dots, \mathcal{X}_{*P}(t)$. A key step in the derivation is to compute the probability $\mathbf{P}[x_{*1}(t+\Delta t), x_{*2}(t+\Delta t), \dots, x_{*P}(t+\Delta t)|k, \mathcal{X}_{*1}(t), \dots, \mathcal{X}_{*P}(t)]$ which predicts the counts of the output species based on their histories. This is an optimal Bayesian filtering problem. The structure of this filtering problem is identical to the one considered in [16]. In [16], we consider a filtering problem where the state vector evolves according to a CTMP. In that problem, only some elements of the state vector can be observed and the aim is to predict the future values of the observable elements from their past histories. We can therefore apply the method in [16] to the demodulation problem considered in this paper. We remark that although the presentation in [16] states

that the output species come from one voxel, it is the structure of the filtering problem that really matters; in other words, it is not important whether the output species come from one or many voxels.

In order to simplify the notation, we will use the shorthand $\mathcal{X}_{*R}(t)$ to denote the histories $\mathcal{X}_{*1}(t)$, \dots , $\mathcal{X}_{*P}(t)$ from all the receiver voxels; note that the subscript R in $\mathcal{X}_{*R}(t)$ is short for receiver. Let $L_k(t) = \log(\mathbf{P}[k|\mathcal{X}_{*R}(t)])$ be the log-posteriori probability that the k -th symbol has been sent given the histories. In Appendix A, we show that $L_k(t)$ evolves according to:

$$\begin{aligned} \frac{dL_k(t)}{dt} = & \sum_{p=1}^P \left(\left[\frac{dx_{*p}(t)}{dt} \right]_+ \log(\mathbf{E}[n_{R,p}(t)|k, \mathcal{X}_{*R}(t)]) - \right. \\ & \left. g_+(M_p - x_{*p}(t)) \mathbf{E}[n_{R,p}(t)|k, \mathcal{X}_{*R}(t)] \right) \end{aligned} \quad (5)$$

where $\mathbf{E}[n_{R,p}(t)|k, \mathcal{X}_{*R}(t)]$ is the estimated number of signalling molecules in the p -th receiver voxel given k and the histories $\mathcal{X}_{*R}(t)$.

Although the term $\mathbf{E}[n_{R,p}(t)|k, \mathcal{X}_{*R}(t)]$ can be computed by solving an optimal Bayesian filtering problem, its computational complexity is high. Another issue, which is found in the multi-voxel receiver case but not the single-voxel receiver case, is that the estimation of the mean number of signalling molecule in the p -th receiver voxel via $\mathbf{E}[n_{R,p}(t)|k, \mathcal{X}_{*R}(t)]$ requires the history in the p -th receiver voxel as well as other receiver voxels. In other words, the computation of $\mathbf{E}[n_{R,p}(t)|k, \mathcal{X}_{*R}(t)]$ requires communications between receiver voxels, which adds burden to the receiver. We follow our earlier work [15][16] and replace $\mathbf{E}[n_{R,p}(t)|k, \mathcal{X}_{*R}(t)]$ with the prior knowledge $\mathbf{E}[n_{R,p}(t)|k]$, which will be denoted by $\alpha_p(t)$. With this replacement, Eq. (5) becomes:

$$\frac{Z_k(t)}{dt} = \sum_{p=1}^P Z_{k,p}(t) \quad (6)$$

$$Z_{k,p}(t) = \left[\frac{dx_{*p}(t)}{dt} \right]_+ \log(\alpha_p(t)) - g_+(M_p - x_{*p}(t)) \alpha_p(t) \quad (7)$$

We can interpret $Z_{k,p}(t)$ in Eq. (7) as the approximate log-posteriori probability computed using the measurements $x_{*p}(t)$ from the p -th voxel. These approximate log-probabilities are then added up or fused in Eq. (6) to obtain the approximate log-posteriori probability of the receiver.

D. MAP demodulator for the mixed configuration

This section considers the demodulation for the mixed configuration. For the mixed configuration, we assume that the X and X_{*} molecules are allowed to diffuse between the receiver voxels but they are not allowed to leave the receiver. Let D_r be the diffusion coefficient of X_{*} in the receiver voxels. Note

TABLE I
NOTATION AND CHEMICAL SYMBOLS

Symbols	Notation and Value
w	Dimension of one side of a voxel
D	diffusion coefficient of signalling molecules
d	Diffusion rate between neighbouring voxels in the medium
d_r	Diffusion rate between receiver species
g_+	Propensity function constant for the activation reaction (1a)
g_-	Propensity function constant for deactivation reaction (1b)
X	Inactivate receptors
X_*	Active receptors
S	Signalling molecules
P	Number of receiver voxels

that we do not specify the diffusion coefficient of X because it does not enter the ODE for computing log-posteriori probability.

If X and X_* are not allowed to diffuse, i.e. for the partitioned case, then $x_p(t) + x_{*p}(t)$ is a constant for any receiver voxel $p = 1, \dots, P$. However, this condition no longer holds for the mixed configuration. This means that M_p are not parameters of the mixed configuration.

The aim of the demodulation problem is to determine the posteriori probability $\mathbf{P}[k | \mathcal{X}_{*1}(t), \dots, \mathcal{X}_{*P}(t)]$ that the k -th transmitter symbol has been sent given the histories $\mathcal{X}_{*1}(t), \dots, \mathcal{X}_{*P}(t)$. We again use $\mathcal{X}_{*R}(t)$ to denote the histories.

In Appendix B, we derive the optimal demodulation filter:

$$\frac{dL_k(t)}{dt} = \sum_{p=1}^P \left(\left[\frac{dx_{*p}(t)}{dt} \right]_+ \log(\mathbf{E}[x_p(t)n_{R,p}(t) | k, \mathcal{X}_{*,R}(t)]) - g_+ \mathbf{E}[x_p(t)n_{R,p}(t) | k, \mathcal{X}_{*p}(t)] \right) \quad (8)$$

where $\mathbf{E}[x_p(t)n_{R,p}(t) | k, \mathcal{X}_{*,R}(t)]$ is the estimated mean of the product of $x_p(t)$ and $n_{R,p}(t)$ by using the histories. Note that in the partitioned case, we can deduce $x_p(t)$ from $M_p - x_{*p}(t)$ but this is no longer the case for the mixed configuration, hence $x_p(t)$ appears in the above ODE. Note that the expression $x_p(t)n_{R,p}(t)$ is proportional to the rate at which X is activated in the p -th receiver voxel at time t and we can learn from our work in [16] that the activation of X is a source of information for demodulation.

Note also that the diffusion rate $d_r = \frac{D_r}{w^2}$ does not enter explicitly in Eq.(8). However, the diffusion rate d_r indirectly influences the log-posteriori probability computation because the statistical properties of $x_p(t)$ depends on d_r . We will study the impact of d_r on BER numerically in Section V.

In order to avoid solving an optimal Bayesian filtering problem in Eq. (8), we will replace $\mathbf{E}[x_p(t)n_{R,p}(t)|k, \mathcal{X}_{*,R}(t)]$ by $\mathbf{E}[x_p(t)n_{R,p}(t)|k]$, which is denoted by $\beta_{k,p}(t)$. This replacement also removes the need for the voxels to communicate with each other. With this replacement, Eq. (8) becomes:

$$\frac{dL_k(t)}{dt} = \sum_{p=1}^P \left(\left[\frac{dx_{*p}(t)}{dt} \right]_+ \log(\beta_{k,p}(t)) - g_+ \beta_{k,p}(t) \right) \quad (9)$$

This will be the demodulation filter for the k -th symbol for the mixed configuration. Note that the above equation can be considered as the fusion of P approximate log-posteriori probabilities.

Remark 2: Although we have presented the results assuming that the molecular circuit is given by Reactions (1). Our methodology can be used for any molecular circuit. The key to deriving the demodulator is to compute the counterpart of the probability $\mathbf{P}[x_{*1}(t + \Delta t), x_{*2}(t + \Delta t), \dots, x_{*P}(t + \Delta t)|k, \mathcal{X}_{*1}(t), \dots, \mathcal{X}_{*P}(t)]$ when different molecular circuits are used. In words, this probability can be stated as: $\mathbf{P}[\text{counts of all the output species from all receiver voxel at time } t + \Delta t|k, \text{ histories of the counts of all the output species from all receiver voxel up to time } t]$. We can again use the method in [16] to determine this probability.

Remark 3: It is possible for a receiver to have both mixed and partitioned configurations. The derivation of the filters for this case is straightforward. We use the summand of the RHS of Eq. (5) for those voxels that are partitioned and that of Eq. (8) for those voxels that are mixed. After that we sum up the log-posteriori probability contributed by each voxel.

We mentioned earlier that there is no loss of generality to consider all P voxels being connected. If the receiver does not form one connected component, then we can compute the log-posteriori probability for each connected component and sum them up. \square

V. NUMERICAL EXAMPLES

This section presents numerical results to understand the performance of the partitioned and mixed configurations. We first describe the methodology and then the results.

A. Methodology

We assume that the size of propagation medium is $1\frac{2}{3}\mu\text{m} \times 1\frac{2}{3}\mu\text{m} \times 1\frac{2}{3}\mu\text{m}$ and the size of voxel is $\frac{1}{3}\mu\text{m}^3$ (i.e. $w = \frac{1}{3}\mu\text{m}$). This forms a grid of $5 \times 5 \times 5$ voxels.

We use a 3-tuple to identify the voxels. The transmitter voxel is located at (1,1,1). We will use three different sizes of receiver, consisting of 2, 4 or 6 voxels. When 2 receiver voxels are used, they are located

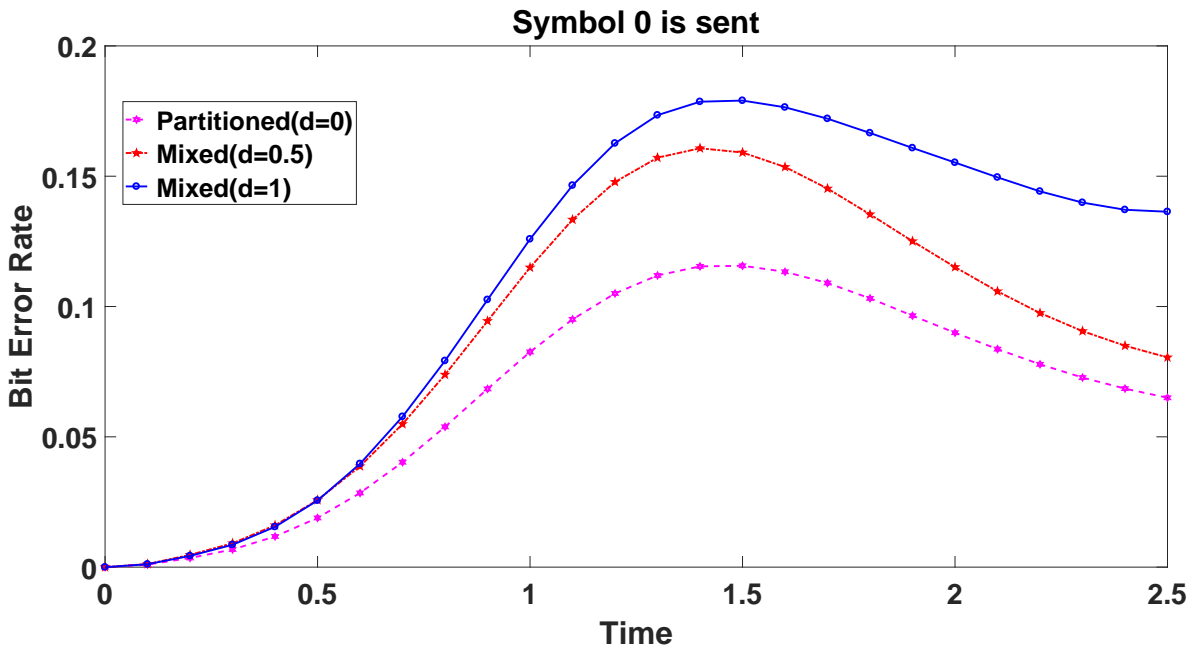


Fig. 5. BER for Mixed and Partitioned for symbol 0.

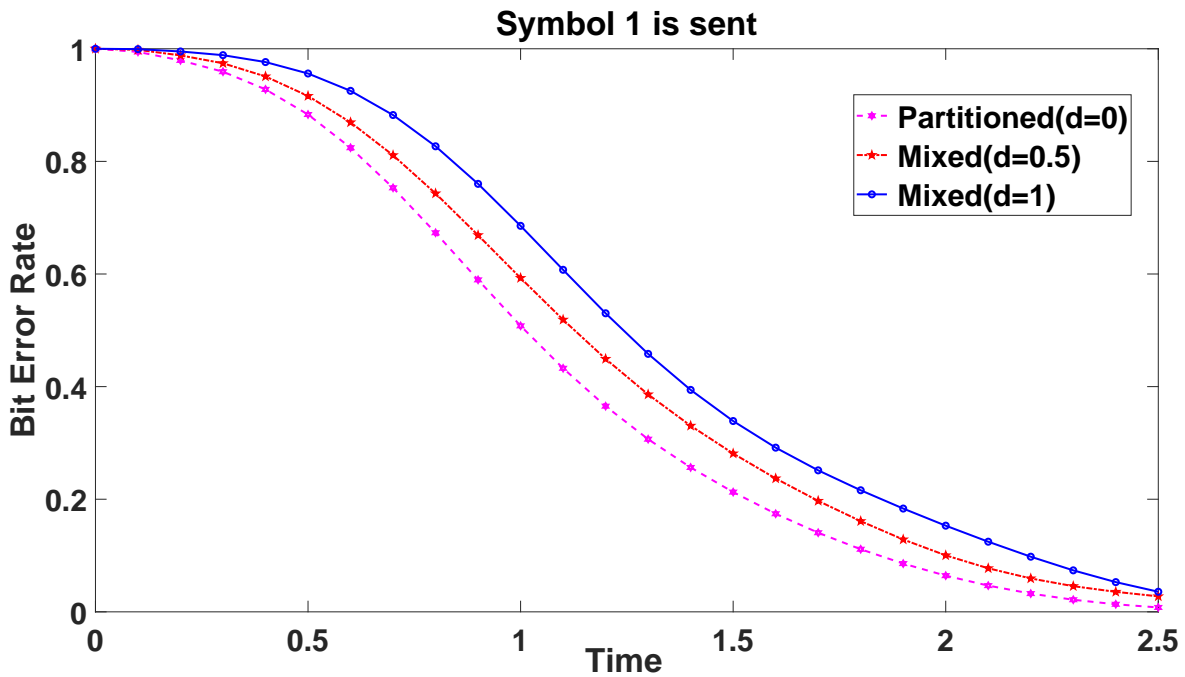


Fig. 6. BER for Mixed and Partitioned for symbol 1.

at (4,5,5) and (5,5,5). For four receiver voxel: (2,5,5), (3,5,5), (4,5,5) and (5,5,5). For six receiver voxel: (5,4,5), (1,5,5), (2,5,5), (3,5,5), (4,5,5) and (5,5,5).

The diffusion coefficient of the propagation medium is $1 \mu\text{m}^2\text{s}^{-1}$. We assume an absorbing boundary condition where signalling molecules may leave the surface of boundary voxel at a rate $\frac{d}{50}$.

The transmitter is assumed to use $K = 2$ symbols. Each symbol is represented by an emission pattern which is generated by a chemical reaction of the form:



where r_k is the rate of production of signalling molecules S when symbol k is transmitted. We assume that symbols 0 and 1 cause, respectively, 10 and 40 signalling molecules to be generated per second on average by the transmitter. The kinetic parameters for the reaction (4a) is 1 and for reaction (4b) is 0.12. The number of receptors will vary from experiment to experiment and will be stated for each experiment.

Unless otherwise stated, the molecular circuits at the receiver voxel is the circuit given in (1).

In the following experiments, for the partitioned configuration, the total number of X and X* in each receiver voxel is given by the parameter M . For the mixed configuration, the value of M should be interpreted as the total number of X and X* in a receiver voxel at the beginning of the simulation. Note that this parameter is common to all receiver voxels.

The parameter D_r is the diffusion coefficient for X and X*. In the experiments, we will use the inter-voxel diffusion rate $d_r = \frac{D_r}{w^2}$ instead. Note that $d_r = 0$ is the same as the partitioned configuration.

Since our interest is in the demodulation performance, we assume that there is no inter-symbol interference (ISI). Note that if ISI is present, we can deal with it using the decision feedback algorithm in our earlier work in [15].

We use Stochastic Simulation Algorithm (SSA) [48] to simulate the CTMP that models both diffusion and reaction of molecules in the system.

The sub-optimal demodulation filter (6) requires the mean $\alpha_{k,p}(t) = E[n_{R,p}(t)|k]$ while the filter (9) requires the mean $\beta_{k,p} = E[x_1(t)n_{R,p}(t)|k]$. We will use SSA simulation to estimate these means by running SSA simulation 500 times and compute the average.

We numerically integrate the sub-optimal demodulation filters to obtain $Z_k(t)$. We use the initial condition $Z_k(0) = 0$ for all k which means that all symbols are equally probable in the system. We will use BER as the performance metric. Each BER value is estimated using 300 independent SSA runs.

B. BER for mixed and partitioned configurations

In this experiment, we study the impact of d_r on the BER. We use $M = 10$ and $P = 2$ for this experiment. We use three values of d_r : 0, 0.5 and 1. The SSA simulations is performed up to time 2.5. Fig. 5 shows the BER for Symbol 0 for these three values of d_r ; and Fig. 6 is for Symbol 1. It can be seen that a lower d_r leads to a lower BER. In particular, the partitioned configuration leads to the lowest BER.

C. BER for different values of diffusion coefficient

The aim of this experiment is to further study the impact of diffusion of the receiver species on BER. We choose $M = 10$ and $P = 2$. We vary d_r from 0 to 1 with an increment of 0.1. We used the BER at time 2.5 for comparison. Figs. 7 and 8 show how BER varies with d_r for, respectively, Symbols 0 and 1. It shows that BER increases monotonically with d_r .

We can consider the partitioned configuration as perfect isolation of receptors into clusters where there is a cluster per voxel and the mixed configuration as imperfect isolation where larger values of d_r means farther away from perfect isolation. The results in this section show that our demodulator offers a gradual degradation in performance with d_r .

In our earlier work [40] we find that the receiver signal $x_{*p}(t)$ for the mixed configuration is noisier than that of the partitioned configuration. This can be understood as follows. For the partitioned configuration, there are two sources of noise: the variation in the number of signalling molecules in the voxel and the stochastic variations due to the reactions (1). However, for the mixed configuration, there is an additional source of noise which is due to the movement of X_* between voxels. The higher signal variance for the mixed configuration leads to a degradation in performance.

D. Impact of the number of receiver voxels with fixed M

This section studies the impact of the number of receiver voxels on BER for partitioned configuration. We maintain $M = 10$ and we use three different receivers, with 2, 4 and 6 voxels. The total number of receptors for these receivers are therefore 20, 40 and 60 respectively. Figs. 9 and 10 show that BER for Symbols 0 and 1 over time. It shows that in general, a higher number of voxels will lead to a lower BER.

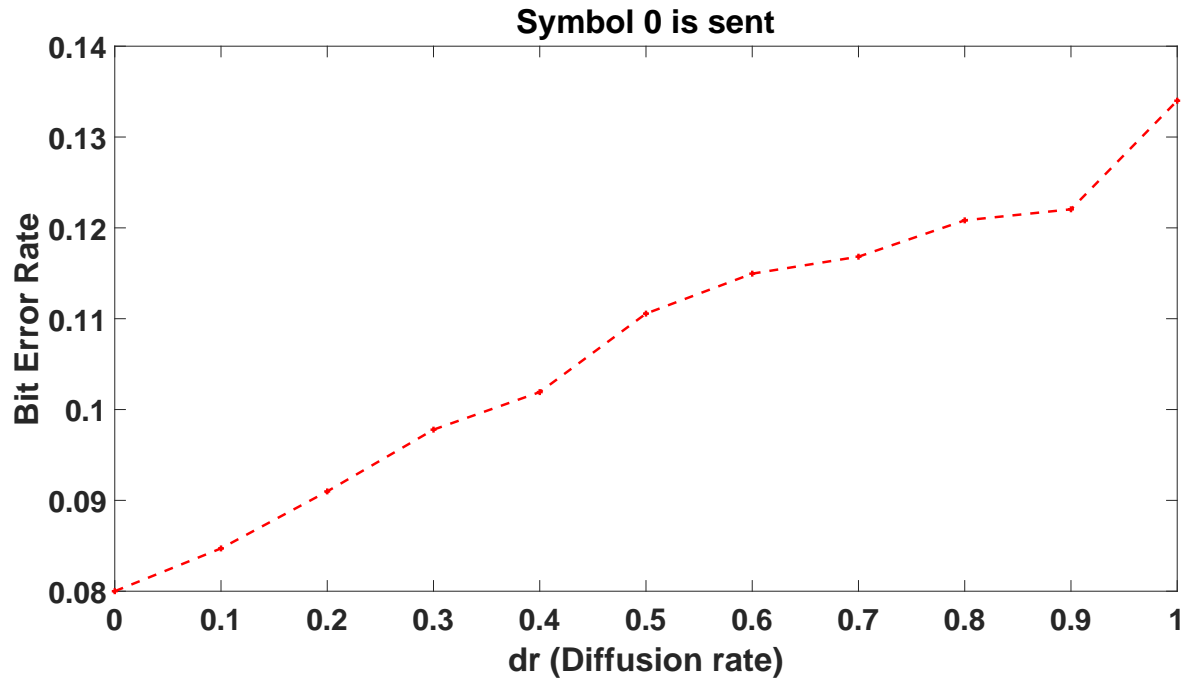


Fig. 7. BER for different values of diffusion coefficient for symbol 0.

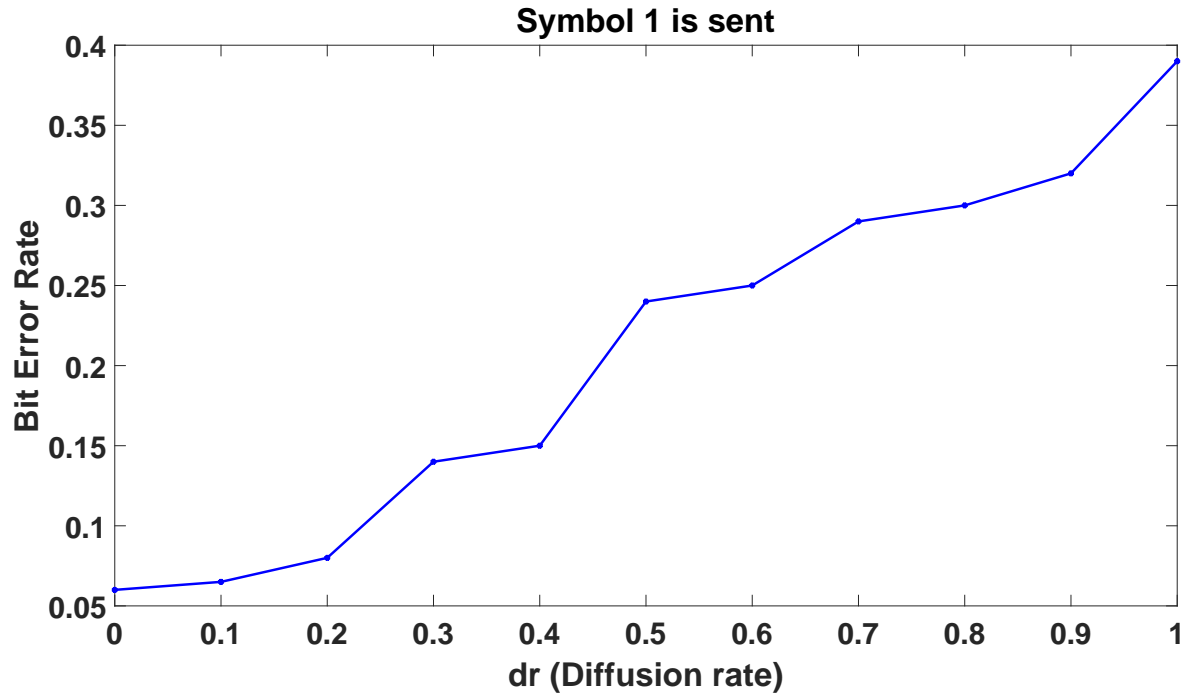


Fig. 8. BER for different values of diffusion coefficient for symbol 1.

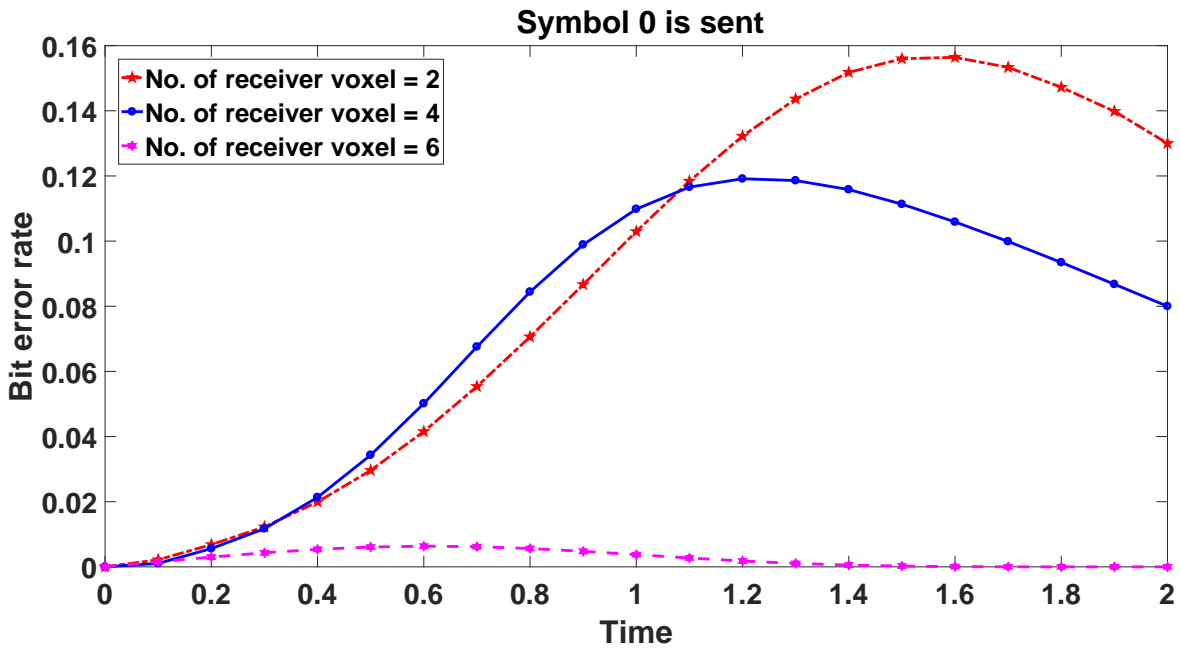


Fig. 9. BER for different number of voxels for symbol 0

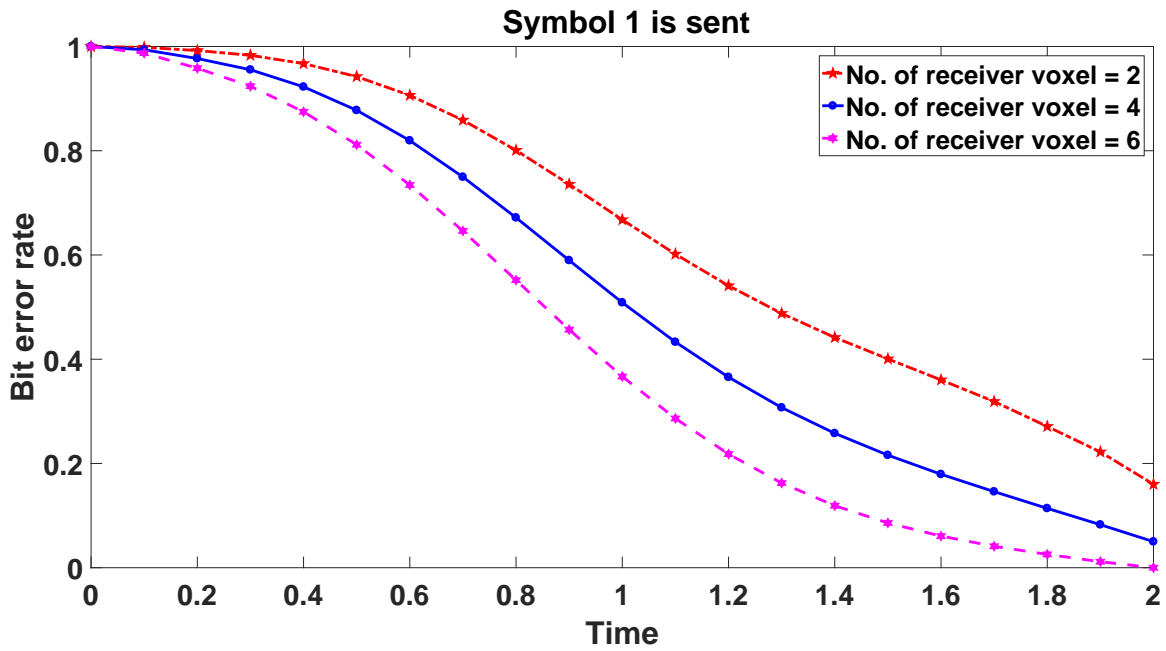


Fig. 10. BER for different number of voxels for symbol 1

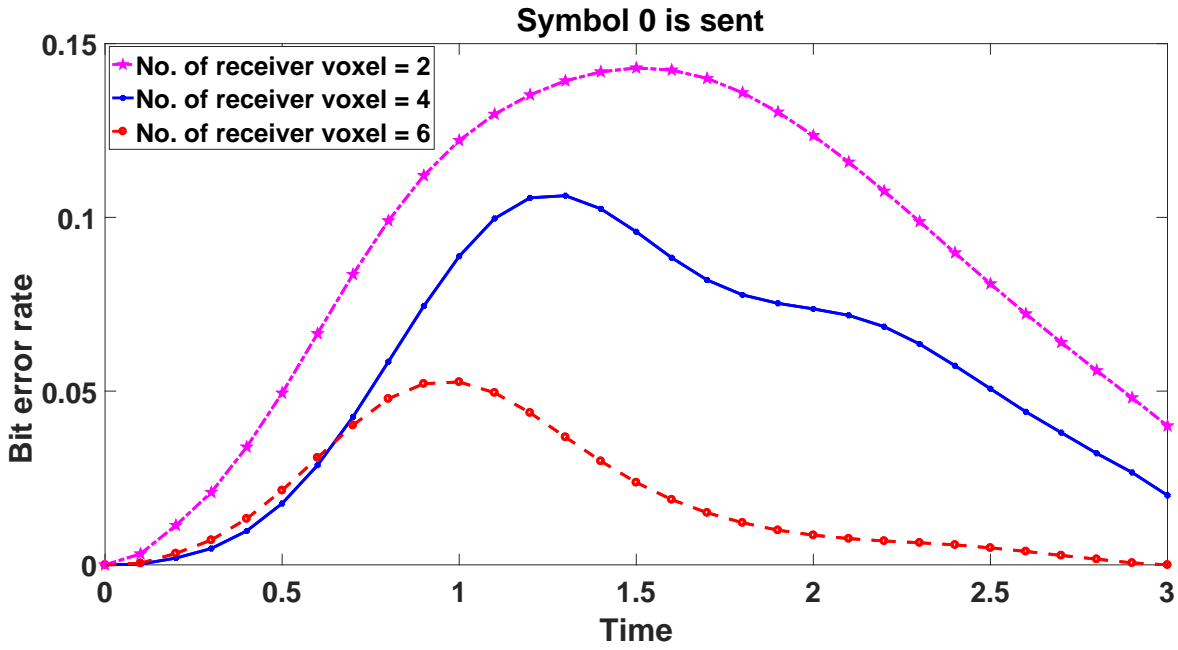


Fig. 11. BER for symbol 0 for different number of voxels when total number of receptor for all receiver voxels i.e. M is fix

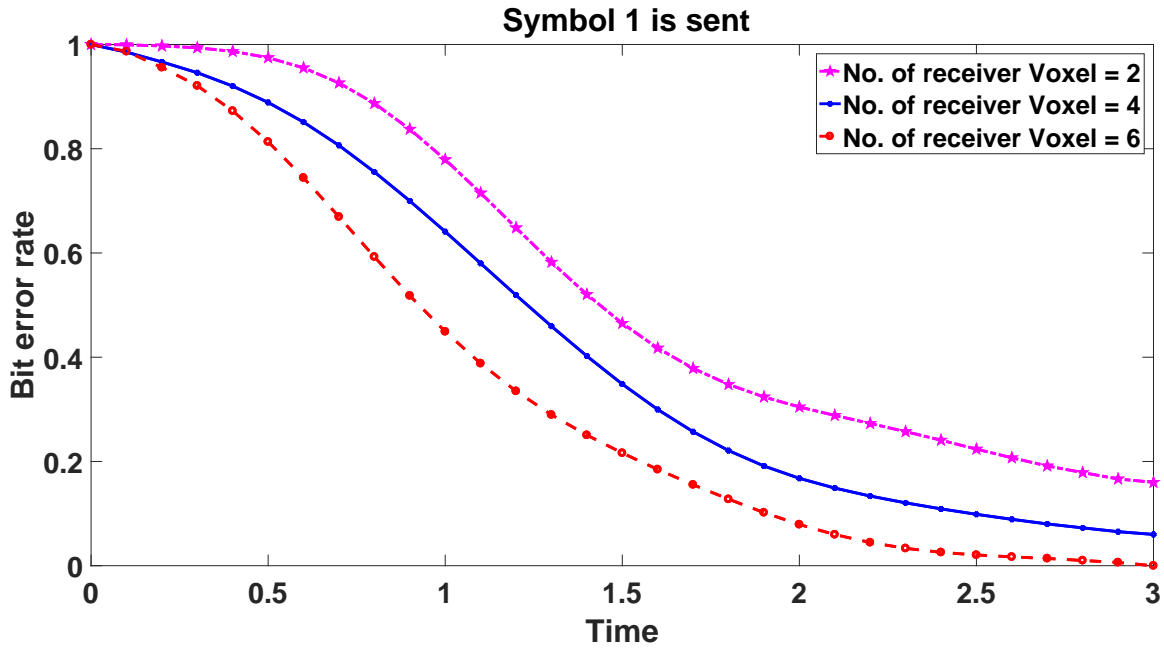


Fig. 12. BER for symbol 1 for different number of voxels when total number of receptor for all receiver voxels i.e. M is fix.

E. Impact of the number of receiver voxels with a fixed total number of receptors

This section studies the impact of the number of receiver voxels on BER. We use three different number of voxels per receiver, namely 2, 4 and 6 voxels. We maintain the total number of receptors in each receiver at 60. Therefore, the number of receptors per voxel for the three receivers are 30, 15 and 10. Figs. 11 and 12 show that BER for Symbols 0 and 1 over time. It shows that in general, a higher number of voxels will lead to a lower BER.

F. BER using a different molecular receiver circuit

All the above experiments have been carried out with the receiver molecular circuit in (1). In this experimnt, we use the following molecular circuit which was used in our earlier work [16]:



where E represent an unbound receptor with two binding sites. In forward reaction (11), E can bind with S molecule to form the complex $C_{[1]}$ whereas in forward reaction (12), $C_{[1]}$ can bind with S molecule to form the complex $C_{[2]}$. Furthermore, $\tilde{\lambda}_1$, μ_1 , $\tilde{\lambda}_2$ and μ_2 are reaction rate constants. The complex $C_{[2]}$ is chosen as the output species. We assume $M = 2$ and $P = 2$. All other parameters remain the same. We use three values of d_r : 0, 0.5 and 1. Figs. 13 and 14 show the BER for, respectively, Symbols 0 and 1. We witness the same trend as before where the BER increases with d_r .

VI. CONCLUSIONS AND FUTURE WORK

This paper considers the demodulation in a molecular communication system where the receiver can be in the partitioned or mixed configuration. We derive the MAP demodulator for both configurations. Our numerical experiment shows that partitioning, or a small diffusion coefficient for the receiver species, can lead to a lower BER. The use of partitioning does not seem to have been studied before so this leads to a new degree of freedom to improve the performance of molecular communication.

This paper models the shape of a receiver by using multiple voxels. This can be considered as using the finite difference method to model the shape of a receiver. The finite difference method is a very basic method to model the shape of 3-dimensional objects. The modern approach is based on finite element or similar methods. We see this as an interesting future direction. The diffusion of molecules in the finite

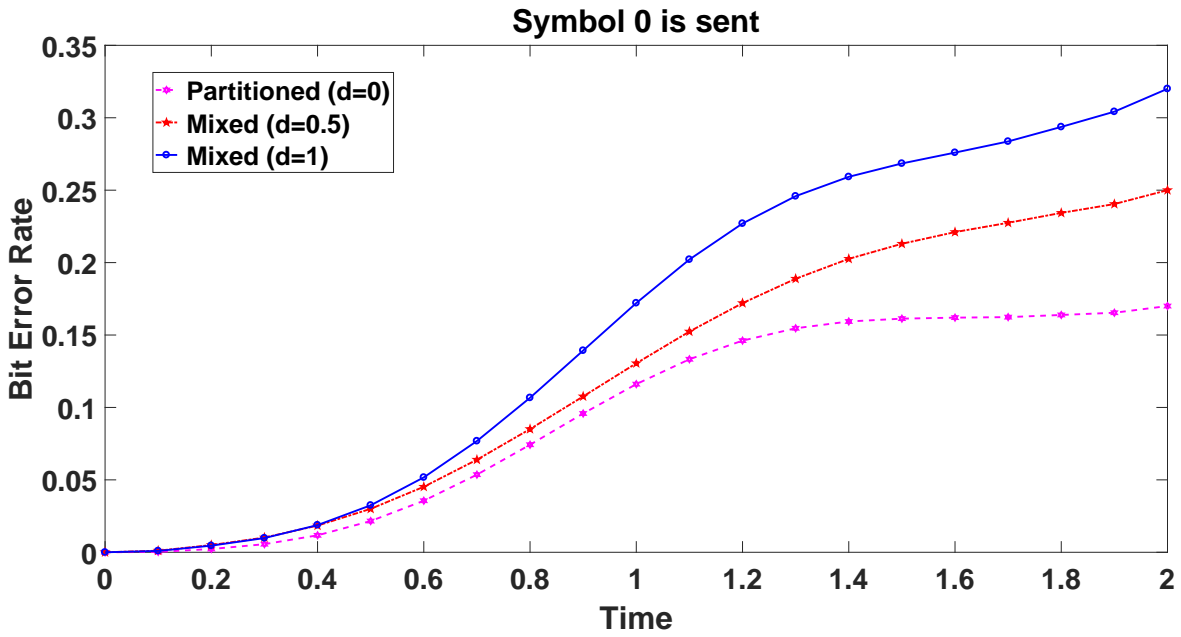


Fig. 13. BER for Mixed and Partitioned for symbol 0

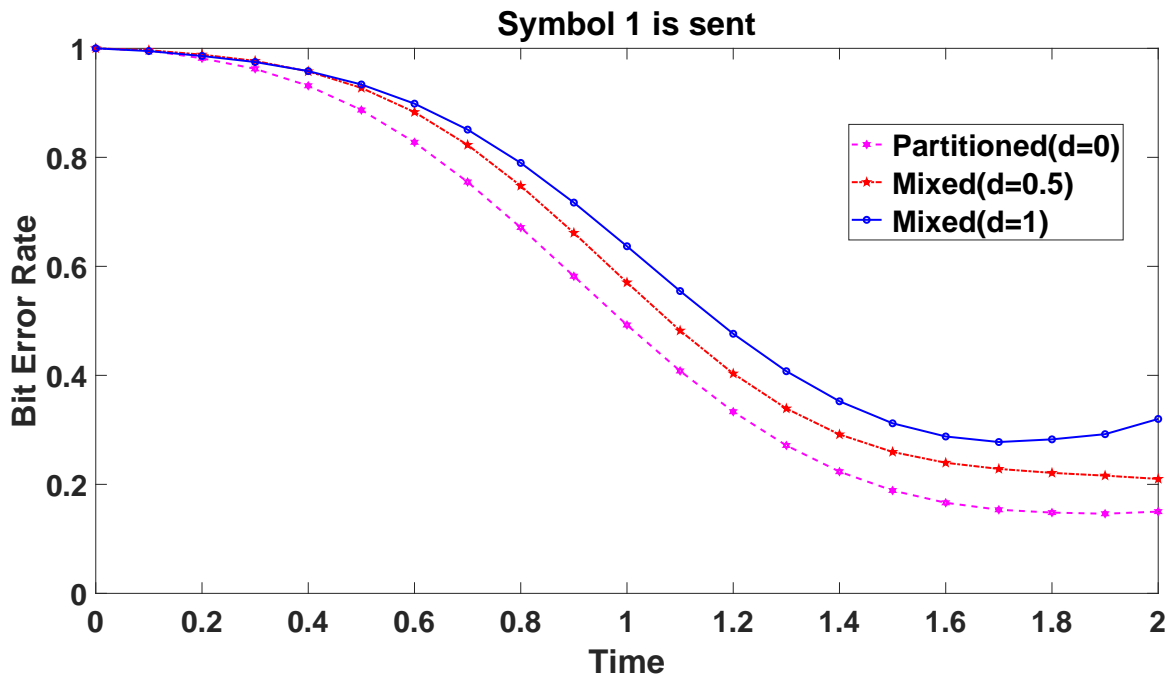


Fig. 14. BER for Mixed and Partitioned for symbol 1

element setting can possibly be handled by the method in [49]. However, reaction-diffusion setting is a lot more complicated than the pure diffusion case. This is because RDME is fundamentally a spatially discrete method to approximate the behaviour of the fine grained Smoluchowski equation [43]. This approximation is only accurate if the discretisation length scale is chosen correctly [50]. Fortunately, there is some recent work on using RDME on an unstructured mesh [50], [51]. Since our demodulator design is based on RDME, these recent work will allow us to extend our work to unstructured mesh to better model the 3-dimensional shape of the receiver.

REFERENCES

- [1] I. Akyildiz, F. Brunetti, and C. Blázquez, “Nanonetworks: A new communication paradigm,” *Computer Networks*, vol. 52, pp. 2260–2279, 2008.
- [2] T. Nakano, T. Suda, Y. Okaie, M. J. Moore, and A. V. Vasilakos, “Molecular Communication Among Biological Nanomachines: A Layered Architecture and Research Issues,” *NanoBioscience, IEEE Transactions on*, vol. 13, no. 3, pp. 169–197, 2014.
- [3] I. F. Akyildiz, M. Pierobon, S. Balasubramaniam, and Y. Koucheryavy, “The internet of bio-nano things,” *IEEE Communications Magazine*, vol. 53, no. 3, pp. 32–40, 2015.
- [4] N. Farsad, H. B. Yilmaz, A. Eckford, C.-B. Chae, and W. Guo, “A comprehensive survey of recent advancements in molecular communication,” *IEEE Communications Surveys & Tutorials*, vol. 18, no. 3, pp. 1887–1919, 2016.
- [5] M. Pierobon and I. Akyildiz, “A physical end-to-end model for molecular communication in nanonetworks,” *IEEE JOURNAL ON SELECTED AREAS IN COMMUNICATIONS*, vol. 28, no. 4, pp. 602–611, 2010.
- [6] D. Kilinc and O. B. Akan, “Receiver design for molecular communication,” *IEEE Journal on Selected Areas in Communications*, vol. 31, no. 12, pp. 705–714, 2013.
- [7] M. U. Mahfuz, D. Makrakis, and H. T. Mouftah, “A comprehensive analysis of strength-based optimum signal detection in concentration-encoded molecular communication with spike transmission,” *IEEE transactions on nanobioscience*, vol. 14, no. 1, pp. 67–83, 2015.
- [8] V. Jamali, A. Ahmadzadeh, and R. Schober, “On the design of matched filters for molecule counting receivers,” *IEEE Communications Letters*, vol. 21, no. 8, pp. 1711–1714, 2017.
- [9] S. K. Tiwari and P. K. Upadhyay, “Estimate-and-forward relaying in diffusion-based molecular communication networks: Performance evaluation and threshold optimization,” *IEEE Transactions on Molecular, Biological and Multi-Scale Communications*, vol. 3, no. 3, pp. 183–193, 2017.
- [10] Y. Fang, A. Noel, N. Yang, A. W. Eckford, and R. A. Kennedy, “Convex optimization of distributed cooperative detection in multi-receiver molecular communication,” *IEEE Transactions on Molecular, Biological and Multi-Scale Communications*, vol. 3, no. 3, pp. 166–182, 2017.
- [11] A. Noel, K. C. Cheung, and R. Schober, “Improving receiver performance of diffusive molecular communication with enzymes,” *IEEE Transactions on NanoBioscience*, vol. 13, no. 1, pp. 31–43, 2014.
- [12] —, “Optimal receiver design for diffusive molecular communication with flow and additive noise,” *IEEE transactions on nanobioscience*, vol. 13, no. 3, pp. 350–362, 2014.
- [13] M. Farahnak-Ghazani, G. Aminian, M. Mirmohseni, A. Gohari, and M. Nasiri-Kenari, “On medium chemical reaction in diffusion-based molecular communication: a two-way relaying example,” *IEEE Transactions on Communications*, vol. 67, no. 2, pp. 1117–1132, 2019.
- [14] A. Mugler, F. Tostevin, and P. R. Ten Wolde, “Spatial partitioning improves the reliability of biochemical signaling,” *Proceedings of the National Academy of Sciences*, p. 201218301, 2013.

- [15] C. T. Chou, "A markovian approach to the optimal demodulation of diffusion-based molecular communication networks," *IEEE Transactions on Communications*, vol. 63, no. 10, pp. 3728–3743, 2015.
- [16] H. Awan and C. T. Chou, "Generalized solution for the demodulation of reaction shift keying signals in molecular communication networks," *IEEE Transactions on Communications*, vol. 65, no. 2, pp. 715–727, 2017.
- [17] S. Hiyama and Y. Moritani, "Molecular communication: Harnessing biochemical materials to engineer biomimetic communication systems," *Nano Communication Networks*, vol. 1, no. 1, pp. 20–30, May 2010.
- [18] T. Nakano, M. J. Moore, F. Wei, A. V. Vasilakos, and J. Shuai, "Molecular Communication and Networking: Opportunities and Challenges," *IEEE Transactions on Nanobioscience*, vol. 11, no. 2, pp. 135–148, 2012.
- [19] H. ShahMohammadian, G. G. Messier, and S. Magierowski, "Optimum receiver for molecule shift keying modulation in diffusion-based molecular communication channels," *Nano Communication Networks*, vol. 3, no. 3, pp. 183–195, Sep. 2012.
- [20] M. Kuran, H. Yilmaz, T. Tugcu, and I. Akyildiz, "Modulation Techniques for Communication via Diffusion in Nanonetworks," in *Communications (ICC), 2011 IEEE International Conference on*, 2011, pp. 1–5.
- [21] M. Mahfuz, D. Makrakis, and H. Mouftah, "On the characterization of binary concentration-encoded molecular communication in nanonetworks," *Nano Communication Networks*, vol. 1, pp. 289–300, 2010.
- [22] H. Awan and C. T. Chou, "Improving the capacity of molecular communication using enzymatic reaction cycles," *IEEE transactions on nanobioscience*, vol. 16, no. 8, pp. 744–754, 2017.
- [23] —, "Impact of receiver molecular circuits on the performance of reaction shift keying," in *Proceedings of the Second Annual International Conference on Nanoscale Computing and Communication*, ser. NANOCOM' 15. New York, NY, USA: ACM, 2015, pp. 2:1–2:6. [Online]. Available: <http://doi.acm.org/10.1145/2800795.2800798>
- [24] M. U. Mahfuz, D. Makrakis, and H. T. Mouftah, "Strength-based optimum signal detection in concentration-encoded pulse-transmitted OOK molecular communication with stochastic ligand-receptor binding," *Simulation Modelling Practice and Theory*, vol. 42, pp. 189–209, 2014.
- [25] M. Pierobon and I. F. Akyildiz, "Noise Analysis in Ligand-Binding Reception for Molecular Communication in Nanonetworks," *IEEE Transactions on Signal Processing*, vol. 59, no. 9, pp. 4168–4182, 2011.
- [26] —, "Diffusion-based Noise Analysis for Molecular Communication in Nanonetworks," *IEEE Transactions on Signal Processing*, vol. 59, no. 6, pp. 2532–2547, 2011.
- [27] C. T. Chou, "Extended master equation models for molecular communication networks," *IEEE Transactions on Nanobioscience*, vol. 12, no. 2, pp. 79–92, 2013, doi:10.1109/TNB.2013.2237785.
- [28] H. Awan, "Reducing the effect of reaction rate constants on the performance of molecular communication networks," in *Proceedings of the 3rd ACM International Conference on Nanoscale Computing and Communication*. ACM, 2016, p. 8.
- [29] C. T. Chou, "Maximum A-Posteriori Decoding for Diffusion-Based Molecular Communication Using Analog Filters," *Nanotechnology, IEEE Transactions on*, vol. 14, no. 6, pp. 1054–1067, Nov. 2015.
- [30] P. J. Thomas and A. W. Eckford, "Capacity of a simple intercellular signal transduction channel," *IEEE Transactions on information Theory*, vol. 62, no. 12, pp. 7358–7382, 2016.
- [31] G. Aminian, M. Farahnak-Ghazani, M. Mirmohseni, M. Nasiri-Kenari, and F. Fekri, "On the capacity of point-to-point and multiple-access molecular communications with ligand-receptors," *IEEE Transactions on Molecular, Biological and Multi-Scale Communications*, vol. 1, no. 4, pp. 331–346, 2015.
- [32] C. T. Chou, "Molecular communication networks with general molecular circuit receivers," in *ACM The First Annual International Conference on Nanoscale Computing and Communication*. New York, New York, USA: ACM Press, 2014, pp. 1–9.
- [33] M. Kuscü and O. B. Akan, "Maximum likelihood detection with ligand receptors for diffusion-based molecular communications in internet of bio-nano things," *IEEE transactions on nanobioscience*, vol. 17, no. 1, pp. 44–54, 2018.

- [34] C. T. Chou, "Impact of Receiver Reaction Mechanisms on the Performance of Molecular Communication Networks," *IEEE Transactions on Nanotechnology*, vol. 14, no. 2, pp. 304–317, Mar. 2015.
- [35] B. Atakan and O. B. Akan, "Deterministic capacity of information flow in molecular nanonetworks," *Nano Communication Networks*, vol. 1, no. 1, pp. 31–42, May 2010.
- [36] A. Einolghozati, M. Sardari, A. Beirami, and F. Fekri, "Capacity of discrete molecular diffusion channels." *ISIT*, pp. 723–727, 2011.
- [37] M. Pierobon and I. Akyildiz, "Capacity of a Diffusion-Based Molecular Communication System With Channel Memory and Molecular Noise," *Information Theory, IEEE Transactions on*, vol. 59, no. 2, pp. 942–954, 2013.
- [38] G. Aquino, D. Clausznitzer, S. Tollis, and R. G. Endres, "Optimal receptor-cluster size determined by intrinsic and extrinsic noise," *Physical Review E*, vol. 83, no. 2, p. 021914, 2011.
- [39] G. Chatterjee, N. Dalchau, R. A. Muscat, A. Phillips, and G. Seelig, "A spatially localized architecture for fast and modular dna computing," *Nature nanotechnology*, vol. 12, no. 9, p. 920, 2017.
- [40] M. U. Riaz, H. Awan, and C. T. Chou, "Using spatial partitioning to reduce receiver signal variance in diffusion-based molecular communication," in *Proceedings of the 5th ACM International Conference on Nanoscale Computing and Communication*. ACM, 2018, p. 12.
- [41] C. Gardiner, *Stochastic methods*. Springer, 2010.
- [42] C. T. Chou, "Designing molecular circuit for approximate maximum a posteriori demodulation of concentration modulated signals," *arXiv preprint arXiv:1808.01543*, 2018.
- [43] M. v. Smoluchowski, "Versuch einer mathematischen theorie der koagulationskinetik kolloider lösungen," *Zeitschrift für physikalische Chemie*, vol. 92, no. 1, pp. 129–168, 1918.
- [44] R. Erban, J. Chapman, and P. Maini, "A practical guide to stochastic simulations of reaction-diffusion processes," *arXiv preprint arXiv:0704.1908*, 2007.
- [45] D. Del Vecchio and R. M. Murray, *Biomolecular Feedback Systems*. Princeton University Press, 2014.
- [46] A. Noel, K. C. Cheung, R. Schober, D. Makrakis, and A. Hafid, "Simulating with accord: Actor-based communication via reaction–diffusion," *Nano Communication Networks*, vol. 11, pp. 44–75, 2017.
- [47] S. Hellander, A. Hellander, and L. Petzold, "Mesoscopic-microscopic spatial stochastic simulation with automatic system partitioning," *The Journal of chemical physics*, vol. 147, no. 23, p. 234101, 2017.
- [48] D. Gillespie, "Exact stochastic simulation of coupled chemical reactions," *The journal of physical chemistry*, 1977.
- [49] S. A. Isaacson and C. S. Peskin, "Incorporating diffusion in complex geometries into stochastic chemical kinetics simulations," *SIAM Journal on Scientific Computing*, vol. 28, no. 1, pp. 47–74, 2006.
- [50] S. Hellander and L. Petzold, "Reaction rates for a generalized reaction-diffusion master equation," *Physical Review E*, vol. 93, no. 1, p. 013307, 2016.
- [51] S. A. Isaacson and Y. Zhang, "An unstructured mesh convergent reaction–diffusion master equation for reversible reactions," *Journal of Computational Physics*, vol. 374, pp. 954–983, 2018.

APPENDIX A

PARTITIONED CONFIGURATION

In this appendix we show how the demodulation filter Eq.(5) can be derived. We first explain how the case for $P = 2$ can be derived and then explain how it can be generalised.

We follow the method in [16]. The first step of the derivation is determine the probability $\mathbf{P}[x_{*1}(t + \Delta t), x_{*2}(t + \Delta t) | k, \mathcal{X}_{*2}(t), \mathcal{X}_{*2}(t)]$. In [16] we present an algorithm to write down the expression of this

probability by identifying all the reactions that can change the count of the output species, i.e. X_{*1} and X_{*2} . By using the algorithm in [16], we can show that:

$$\begin{aligned}
& \mathbf{P}[x_{*1}(t + \Delta t), x_{*2}(t + \Delta t) | k, \mathcal{X}_{*2}(t), \mathcal{X}_{*2}(t)] = \\
& \delta(x_{*1}(t + \Delta t) = x_{*1}(t) + 1, x_{*2}(t + \Delta t) = x_{*2}(t))Q_{1,a} + \\
& \delta(x_{*1}(t + \Delta t) = x_{*1}(t) - 1, x_{*2}(t + \Delta t) = x_{*2}(t))Q_{1,d} + \\
& \delta(x_{*1}(t + \Delta t) = x_{*1}(t), x_{*2}(t + \Delta t) = x_{*2}(t) + 1)Q_{2,a} + \\
& \delta(x_{*1}(t + \Delta t) = x_{*1}(t), x_{*2}(t + \Delta t) = x_{*2}(t) - 1)Q_{2,d} + \\
& \delta(x_{*1}(t + \Delta t) = x_{*1}(t), x_{*2}(t + \Delta t) = x_{*2}(t))Q_0
\end{aligned} \tag{13}$$

where $\delta()$ is an indicator function which takes the value of 1 if all the conditions within $()$ are true, otherwise its value is 0. In addition, we have:

$$\begin{aligned}
Q_{1,a} &= g_+(M_1 - x_{*1}(t))E[n_{R,1}(t) | k, \mathcal{X}_{*1}(t), \mathcal{X}_{*2}(t)]\Delta t \\
Q_{1,d} &= g_-x_{*1}(t)\Delta t \\
Q_{2,a} &= g_+(M_1 - x_{*1}(t))E[n_{R,2}(t) | k, \mathcal{X}_{*1}(t), \mathcal{X}_{*2}(t)]\Delta t \\
Q_{2,d} &= g_-x_{*2}(t)\Delta t \\
Q_0 &= 1 - (Q_{1,a} + Q_{1,d} + Q_{2,a} + Q_{2,d})
\end{aligned} \tag{14}$$

Note that the term $Q_{1,a}$ in Eq. (13) corresponds to the case where the activation reaction (1a) takes place in receiver voxel 1 because $\delta(x_{*1}(t + \Delta t))$ is one greater than $x_{*1}(t)$. The subscripts 1 and a in $Q_{1,a}$ refer to receiver voxel 1 and activation reaction. Similarly, $Q_{1,d}$ refers to deactivation reaction in voxel 1. The terms $Q_{2,a}$ and $Q_{2,d}$ are for voxel 2. Lastly, the term Q_0 corresponds to no reactions taking place.

The next step is to derive the ODE which shows how the log-posteriori probability $L_k(t)$ evolves over time. From [16], we have:

$$\frac{dL_k(t)}{dt} = \lim_{\Delta t \rightarrow 0} \frac{\log(\mathbf{P}[x_{*1}(t + \Delta t), x_{*2}(t + \Delta t) | k, \mathcal{X}_{*R}(t)])}{\Delta t} + L'(t) \tag{15}$$

where $L'(t)$ is a term independent of symbol k . Since $L_k(t)$ does not appear on the RHS of the above equation and $L'(t)$ adds the same contribution to all $L_k(t)$ for all $k = 0, \dots, K - 1$, we can therefore ignore $L'(t)$ for the purpose of demodulation since it is the relative (rather than the absolute) magnitude of $L_k(t)$ which is needed for demodulation.

By dropping $L'(t)$, we can compute the shifted version of the log-posteriori probability $L_k(t)$. For conciseness, we use $L_k(t)$ to denote the shifted version of the log-posteriori probability. We therefore have:

$$\frac{dL_k(t)}{dt} = \lim_{\Delta t \rightarrow 0} \frac{\log(\mathbf{P}[x_{*p}(t + \Delta t)|k, \mathcal{X}_{*p}(t)])}{\Delta t} \quad (16)$$

The next step is to substitute Eq. (13) into Eq. (16). After some lengthy manipulations, we arrive at:

$$\begin{aligned} \frac{dL_k(t)}{dt} = & \sum_{p=1}^2 \left(\left[\frac{dx_{*p}(t)}{dt} \right]_+ \log(\mathbf{E}[n_{R,p}(t)|k, \mathcal{X}_{*R}(t)]) - \right. \\ & \left. g_+(M_p - x_{*p}(t)) \mathbf{E}[n_p(t)|k, \mathcal{X}_{*R}(t)] \right) \end{aligned} \quad (17)$$

which is Eq. (5) for the case of $P = 2$.

For general P , there will be $(2P + 1)$ terms in the counterpart of Eq. (13). Out of these $(2P + 1)$ terms, $2P$ of them are $Q_{p,a}$ and $Q_{p,d}$ for $p = 1, \dots, P$. The last term is Q_0 , which equals to $1 - \sum_{p=1}^P (Q_{p,a} + Q_{p,d})$. After writing down the counterpart of Eq. (13) for P voxels, we can follow the above procedure to derive Eq. (5).

APPENDIX B

MIXED CONFIGURATION

In this appendix we derive the demodulation filter for the mixed configuration for $P = 2$. The derivation in this appendix is similar to that for the partitioned configuration in A.

The first step of the derivation is to determine the probability $\mathbf{P}[x_{*1}(t + \Delta t), x_{*2}(t + \Delta t)|k, \mathcal{X}_{*2}(t), \mathcal{X}_{*2}(t)]$. As mentioned in Appendix A, we can use the method in [16] which is to identify all the reactions that can change the counts of the output species, i.e. X_{*1} and X_{*2} . It is important to point out here that the term *reactions* here takes on a generalized meaning. In the modelling framework of RDME, the diffusion of a species from one voxel to another voxel is considered as a first order chemical reactions [44]. Therefore, when we consider the reactions that can change the counts of X_{*1} and X_{*2} , we will also need to include the diffusion of the X_* species between the voxels. Recall that D_r is the diffusion coefficient of X_* . Let

$d_r = \frac{D}{w^2}$ where w is the length of a voxel edge. By using the algorithm in [16], we have:

$$\begin{aligned}
& \mathbf{P}[x_{*1}(t + \Delta t), x_{*2}(t + \Delta t) | k, \mathcal{X}_{*1}(t), \mathcal{X}_{*2}(t)] = \\
& \delta(x_{*1}(t + \Delta t) = x_{*1}(t) + 1, x_{*2}(t + \Delta t) = x_{*2}(t))Q_{1,a} + \\
& \delta(x_{*1}(t + \Delta t) = x_{*1}(t) - 1, x_{*2}(t + \Delta t) = x_{*2}(t))Q_{1,d} + \\
& \delta(x_{*1}(t + \Delta t) = x_{*1}(t), x_{*2}(t + \Delta t) = x_{*2}(t) + 1)Q_{2,a} + \\
& \delta(x_{*1}(t + \Delta t) = x_{*1}(t), x_{*2}(t + \Delta t) = x_{*2}(t) - 1)Q_{2,d} + \\
& \delta(x_{*1}(t + \Delta t) = x_{*1}(t) - 1, x_{*2}(t + \Delta t) = x_{*2}(t) + 1) \\
& Q_{1 \rightarrow 2} + \delta(x_{*1}(t + \Delta t) = x_{*1}(t) + 1, x_{*2}(t + \Delta t) = \\
& x_{*2}(t) - 1)Q_{2 \rightarrow 1} + \delta(x_{*1}(t + \Delta t) = x_{*1}(t), x_{*2}(t + \Delta t) = \\
& x_{*2}(t))Q_0
\end{aligned} \tag{18}$$

where

$$\begin{aligned}
Q_{1,a} &= g_+ E[x_1(t) n_{R1}(t) | k, \mathcal{X}_{*1}, \mathcal{X}_{*2}(t)] \Delta t \\
Q_{1,d} &= g_- x_{*1}(t) \Delta t \\
Q_{2,a} &= g_+ E[x_2(t) n_{R2}(t) | k, \mathcal{X}_{*1}, \mathcal{X}_{*2}(t)] \Delta t \\
Q_{2,d} &= g_- x_{*2}(t) \Delta t \\
Q_{1 \rightarrow 2} &= d_r x_{*1}(t) \Delta t \\
Q_{2 \rightarrow 1} &= d_r x_{*2}(t) \Delta t \\
Q_0 &= 1 - (Q_{1,a} + Q_{1,d} + Q_{2,a} + Q_{2,d} + Q_{1 \rightarrow 2} + Q_{2 \rightarrow 1})
\end{aligned}$$

The meanings of the terms $Q_{1,a}$, $Q_{1,d}$ etc. are the same as those in Appendix A. The term $Q_{1 \rightarrow 2}$ corresponds to the diffusion of an X_* molecule from receive voxel 1 to receiver voxel 2. Starting with Eq. (18), we can now follow the same procedure mentioned in Appendix A to obtain the demodulation filter (8) for $P = 2$.

Similarly, we can generalise Eq. (18) to general P . We need to include terms $Q_{p,a}$ and $Q_{p,b}$, as well as diffusion terms $Q_{p_1 \rightarrow p_2}$ and $Q_{p_2 \rightarrow p_1}$ between any pairs of receiver voxels p_1 and p_2 which are neighbours. After forming the counterpart of Eq.(18) for P receiver voxels, we can obtain the demodulation filter (8).